10.1002/anie.202214493

Fast Li-ion Storage and Dynamics in TiO_2 Nanoparticle Clusters Probed by Smart Scanning Electrochemical Cell Microscopy

Emmanuel Batsa Tetteh,[a,b] Dimitrios Valavanis,[a] Enrico Daviddi,[a] Xiangdong Xu,[a] Carla Santana Santos,[b] Edgar Ventosa,[c] Daniel Martín-Yerga,*[a] Wolfgang Schuhmann,*[b] and Patrick R. Unwin*[a]

[a] E. B. Tetteh, D. Valavanis, Dr. E. Daviddi, X. Xu, Dr. D. Martín-Yerga, Prof. Dr. P. R. Unwin
Department of Chemistry, University of Warwick; Coventry CV47AL, United Kingdom
E-mail: Daniel.Martin-Yerga@warwick.ac.uk; P.R.Unwin@warwick.ac.uk

[b] E. B. Tetteh, Dr. C. Santana Santos, Prof. Dr. W. Schuhmann
Analytical Chemistry – Center for Electrochemical Sciences (CES), Faculty of Chemistry and Biochemistry
Ruhr University Bochum; Universitätsstr. 150, D-44780 Bochum, Germany
E-mail: wolfgang.schuhmann@rub.de

[c] Prof. Dr. E. Ventosa,
Department of Chemistry; University of Burgos; Pza. Misael Bañuelos s/n, 09001 Burgos Spain

Supporting information for this article is given via a link at the end of the document.

Abstract: Anatase TiO_2 is a promising material for Li-ion (Li^+) batteries with fast charging capability. However, Li^+ (de)intercalation dynamics in TiO_2 remain elusive and reported diffusivities span many orders of magnitude. Here, we develop a smart protocol for scanning electrochemical cell microscopy (SECCM) with *in situ* optical microscopy (OM) to enable the high-throughput charge/discharge analysis of single TiO_2 nanoparticle clusters. Directly probing active nanoparticles revealed that TiO_2 with a size of ~50 nm can store over 30% of the theoretical capacity at an extremely fast charge/discharge rate of ~100 C. This finding of fast Li^+ storage in TiO_2 particles strengthens its potential for fast-charging batteries. More generally, smart SECCM-OM should find wide applications for high-throughput electrochemical screening of nanostructured materials.

Li-ion batteries are the frontrunner technology for high-power and intermediate-scale energy storage used in a broad range of applications, including electric vehicles and portable devices.[1] Anatase TiO_2 is a promising fast-charging material for Li-ion battery anodes with theoretical specific charge capacities competitive with those of graphite electrodes.[2–8] TiO_2 is abundant, inexpensive[6] and shows low volume changes (<4%) during Li^+ (de)intercalation:[9]

$$TiO_2 + xLi^+ + xe^- \rightleftharpoons Li_xTiO_2 \qquad (1)$$

The operating voltage of anatase TiO_2 (ca. 1.75 V vs Li/Li^+)[6] offers a large voltage gap to Li electroplating and subsequent dendrite formation, enhancing safety even during fast charging.[10,11] This operating potential also prevents the decomposition of the electrolyte and the formation of a solid electrolyte interphase (SEI),[11,12] thereby minimizing Li losses by side reactions and increasing cycle life. Although anatase TiO_2 possesses unique merits, its broad use in Li-ion cells is limited by the apparently low Li^+ diffusion coefficient and low electronic conductivity (~10^{-12} S cm^{-1}).[6] Until now, the rate of Li^+ diffusion in TiO_2 has remained elusive, with reported diffusion coefficients varying by many orders of magnitude (10^{-8} – 10^{-18} cm^2 s^{-1}).[13] Moreover, the maximum practical Li^+ intercalation capacity is particle size-dependent due to the slow diffusion, and x in Li_xTiO_2 is capped at 0.5, excluding surface reactions.[4,13] An approach to overcome the diffusion limitations and improve the capacity is nanostructuring, which provides shorter paths for Li^+ diffusion and large pseudo-capacitive charge storage due to the increased surface area.[4]

TiO_2 materials have been mostly studied integrated into composite electrodes with conductive additives and binders, where the intrinsic behaviour of the active material can be obscured by other phenomena originating from the complexity of the electrode.[6,7] New electrochemical characterization techniques that directly probe the active material are necessary to fully understand the dynamics and mechanisms of Li^+ storage in battery materials. Recent advances in single-entity[14] and nanoscale electrochemistry[15] have enabled the study of individual battery particles[16] and local battery processes[17,18] to reveal new insights not accessible by conventional macroscale techniques. Scanning electrochemical cell microscopy (SECCM)[19–22] is a particularly versatile and powerful technique and has been used to study Li^+ intercalation at single $LiMn_2O_4$[16] and $LiFePO_4$[23] particles in aqueous electrolytes. The use of organic solvents in SECCM[24] and its recent implementation in a glovebox,[12,25] has enabled the study of the early stages of SEI formation on graphite[12] and the dynamics of SEI formation on silicon electrodes.[17] Nanoscale kinetic imaging of $Li_4Ti_5O_{12}$ thin-film electrodes also revealed the intrinsic diffusion coefficient of Li^+.[26] *In situ* optical microscopy (OM) with SECCM offers the possibility of directly locating and targeting particles for electrochemical study.[20–28]

Herein, we used SECCM-OM in an Ar-filled glovebox (Figure 1a) to study the fast dynamics of Li^+ (de)intercalation in single anatase TiO_2 nanoparticle clusters through cyclic voltammetry (CV) charging/discharging. The use of transmission and interference reflection microscopy (IRM) offered the ability to view individual particles (down to a few 100 nm in size) simultaneously to the SECCM pipette and meniscus position. In this work, we developed a smart scanning protocol to target a set of selected position coordinates where TiO_2 particles were detected optically, thereby significantly increasing throughput. This approach enabled us to obtain large datasets of individual nanoparticle clusters, and to run multiple charge/discharge cycles at slower voltammetric scan rates than usually required for conventional high-throughput SECCM, which measures particles and support indiscriminately through the electrochemical analysis of a regular array of points (Figure S1).

The hybrid SECCM-OM setup consisted of an inverted optical microscope that focused an LED light source through an objective lens onto the back side of a transparent Au-coated glass coverslip where TiO_2 nanoparticle clusters were deposited for IRM mode. A separate light source was placed at an angle above the system for

10.1002/anie.202214493

transmission mode (Figure S1). The SECCM pipette (Figure S2) was filled with 1 M $LiPF_6$ in 1:1 volume ratio ethylene carbonate (EC) and ethyl methylcarbonate (EMC), and a Ag wire was inserted to act as a quasi-reference counter electrode (QRCE). Voltammetric measurements of the ferrocene (Fc/Fc^+) redox process (+3.25 V vs. Li/Li^+)[12] were used to calibrate the Ag QRCE to the Li/Li^+ scale (Figure S3a). CV on the bare Au surface, within the potential range relevant to Li^+ (de)intercalation at TiO_2, shows a reduction peak originating from traces of H_2O possibly adsorbed on the electrode or in the electrolyte (Figure S3b,c),[29] but this feature largely disappeared after the first voltammetric cycle leaving an inert background for the study of the TiO_2 nanoparticles (Figure S4).

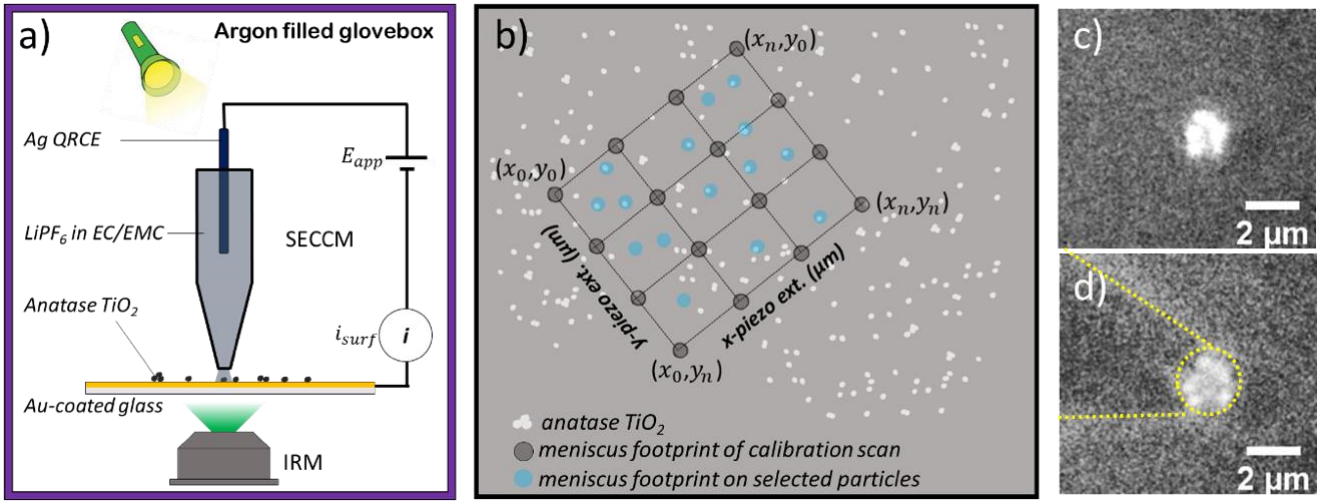

Figure 1. a) Schematic of the setup for SECCM-OM in a glovebox employed for single-entity Li-ion (de)intercalation measurements of TiO_2 nanoparticle clusters. b) Smart scanning protocol to target selected TiO_2 nanoparticles for automated SECCM measurements at a series of specific position coordinates (not drawn to scale). c) Typical *in-situ* IRM image of a single TiO_2 nanoparticle cluster before SECCM tip approach, and d) after meniscus contact from the tip. The yellow dashed lines in (d) highlight the position of the pipet and meniscus.

Anatase TiO_2 (Figure S5 for X-ray diffraction pattern) was drop cast on the Au-coated glass coverslip which served as working electrode for SECCM measurements. A rapid position calibration scan was performed using the SECCM hopping mode with a sparse rectangular grid (Figure 1b). The resulting meniscus footprints, visible in the IRM image, with known (x-y) coordinates served as reference points and the relative positions of particles of interest were used as coordinates to direct the SECCM tip to those particles (Figure S6). Figure 1c shows an *in-situ* IRM image of a TiO_2 nanoparticle cluster before the pipette approach, with the external light source providing visibility of the pipette (Figure 1d) during droplet landing (Movie S1).

Charge/discharge CVs were performed on different-sized TiO_2 nanoparticle clusters. CVs recorded by SECCM on three different TiO_2 clusters and corresponding OM images are presented in Figure 2. The CV response was stable for multiple charge/discharge cycles, indicating that the meniscus wetting of the particle areas was stable. Interestingly, the redox peaks are well defined at a scan rate of 50 mV s^{-1}, about 500 times faster than typically used in battery research.[30] For these 3 cases, the cathodic sweep resulted consistently in a main peak at ~1.5 V vs Li/Li^+, but the CV shape was noticeably different for each cluster, especially in the anodic scan (Li deintercalation): the first cluster (top panel) showed a single sharp peak, whereas the larger second and third clusters showed a much broader response. Since these clusters are assemblies of different nanoparticles, with varying electrical connections and likely with different Li^+ deintercalation kinetics,[16] it is unsurprising to observe a broader response over a larger range of entities. These initial experiments highlight the importance of studying small clusters of TiO_2 (*vide infra*) to map the distribution of activities among similar-sized clusters.

The total charge stored in TiO_2 particles can be separated into three components: faradaic contributions from 1) Li^+ intercalation, 2) surface atom charge-transfer processes, referred to as pseudo-capacitance; and 3) non-faradaic contributions from double layer charging.

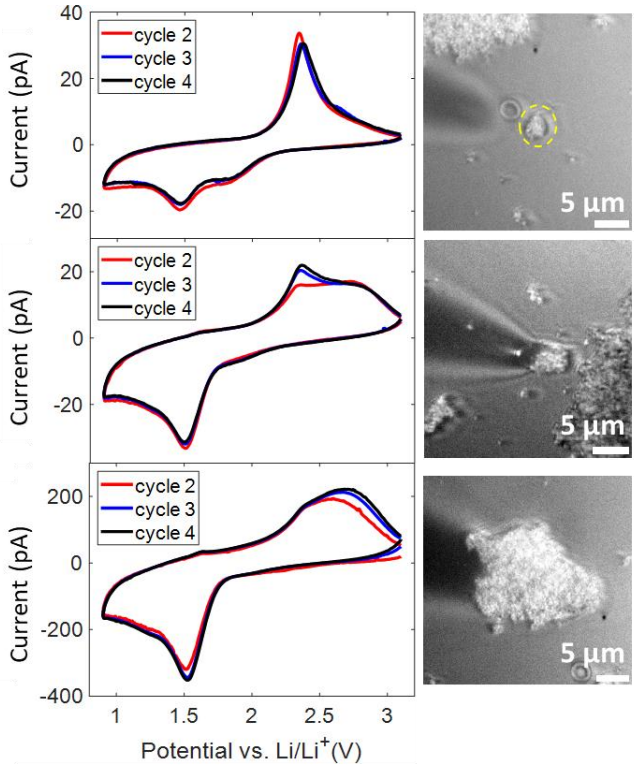

Figure 2. CVs (cycles 2 to 4) at 50 mV s^{-1} from selected TiO_2 clusters with a pipette of 2 µm diameter and the corresponding OM images recorded *in situ*.

10.1002/anie.202214493

To clarify these contributions, we analyzed the dependence of peak current, i_p, on scan rate by recording consecutive CVs at multiple scan rates (20 – 500 mV s^{-1}) on a small cluster (Figure S7). Measured currents obey a power law relationship with scan rates (v):[31]

$$i = av^b \qquad (2)$$

Two limiting conditions are: b = 0.5 (semi-infinite diffusion-limited behavior) and b = 1.0 (capacitive or thin layer response).[5,31] Figure 3 shows: (a) an OM image of a small TiO_2 cluster; and (b) the corresponding CV at 20 mV s^{-1}. A plot of log i_p (peak current) vs log v (Figure 3c) for Li^+ deintercalation revealed a b–value of 0.55 which was calculated from the slope (eq. 2) indicating that Li^+ deintercalation is limited primarily by diffusion through the TiO_2. A b-value of 0.67 was calculated for the cathodic peak (i.e. Li^+ intercalation), however this peak is not devoid of side reactions, which complicates the analysis.[29] Calculated b-values at various potentials for both the cathodic and anodic scans are shown in Figure 3d and 3e, respectively, neglecting the slight systematic peak shift as a function of scan rate (Figure S8). The b-value was close to 0.5 at potentials near the peak currents but approached unity at potentials distant from the peak region. Thus, for the entire scan rate range (20 mV s^{-1} to 500 mV s^{-1}) there is a strong diffusional contribution to (de)intercalation. We estimate the diffusion coefficient of Li^+ in the TiO_2 particles using: [5]

$$i_p = 0.4958nFAC\sqrt{D}\left[\frac{\alpha n_a F}{RT}\right]^{\frac{1}{2}} v^{\frac{1}{2}} \qquad (3)$$

Here, n and n_a are the number of electrons involved in the overall and rate-determining processes, respectively, taken as unity, A is the geometric area of the cluster in the microscope image, v the scan rate, D is the inter-particle diffusion coefficient and C the concentration of Ti^{3+} in the lattice, which is 0.024 mol cm^{-3} for x = 0.5 in Li_xTiO_2, α is taken as 0.5.[5] Note that this estimation ignores changes in particle conductivity,[13] and assumes the "reaction/diffusion layer" thickness at the periphery of the particle is small compared to the particle diameter,[32] which is reasonable under our experimental timescale. Using the slopes of the plots in Figure 3f and Figure S9, the diffusion coefficient was estimated to be 3 × 10^{-15} cm^2 s^{-1} for Li^+ deintercalation and 2 × 10^{-14} cm^2 s^{-1} for Li^+ intercalation. Estimates of the Li^+ diffusivity in anatase TiO_2 vary tremendously depending on the characterization method or the nature of the sample, i.e. single crystal, thin films, nanoporous, or bulk.[4,5,9,13,33–40] Our values are comparable to diffusivities measured recently in anatase thin films.[40] This is because single particles are directly probed within the cluster without any extra contribution to diffusion through porous and composite electrodes. The total charge stored in TiO_2 in our measurements can be estimated and is naturally strongly dependent on the scan rate (Figure S10).

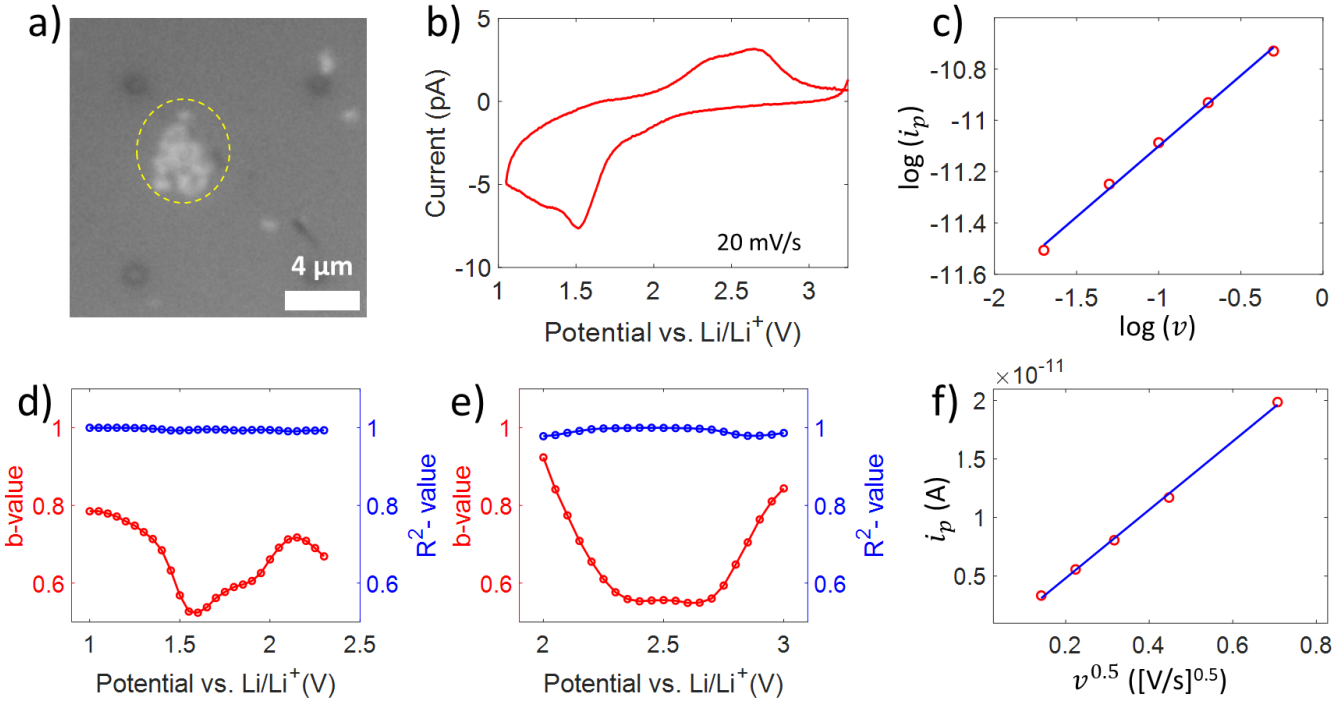

Figure 3. a) IRM image of a single TiO_2 nanoparticle cluster. b) CV at a scan rate (v) of 20 mV s^{-1} recorded with a pipette tip of 3 µm diameter on the cluster marked with a yellow circle in a). c) Plot of log(i_p) vs log(v) for Li^+ deintercalation to estimate the b-value, and b-values as a function of potential for (d) Li^+ intercalation and (e) Li^+ deintercalation. f) Plot of anodic peak current (i_p) vs square root of scan rate (v) to estimate the Li^+ diffusion coefficient. Slope of c) is 0.55 and the slope of f) is 2.9 × 10^{-11} A(V/s) $^{-0.5}$.

Following a position calibration scan, as described earlier, 60 points of interest (including a few points with no visible particles to serve as quality check for the SECCM tip condition during the scan) were extracted by simply clicking on the OM image (Figure 4a and S11), and using the corresponding coordinates as the input for automated SECCM measurements. This protocol increased the chances of landing the SECCM probe on small particles (Movie S2 and S3) and ensured that many particles could be analyzed quickly in a single scan (Figure S12 and S13) to provide statistically relevant data sets. The CVs for this scan were recorded at a scan rate of 50 mV s^{-1}. Another similar scan was performed in a different region (58 points of interest) with the CVs recorded at a scan rate of 100 mV s^{-1} (Figure S14-S16). While particle landings were engaged with a high success, only CVs with well-defined Li (de)intercalation peaks (47 points) were selected for further analysis (Figure S11 and S13).

10.1002/anie.202214493

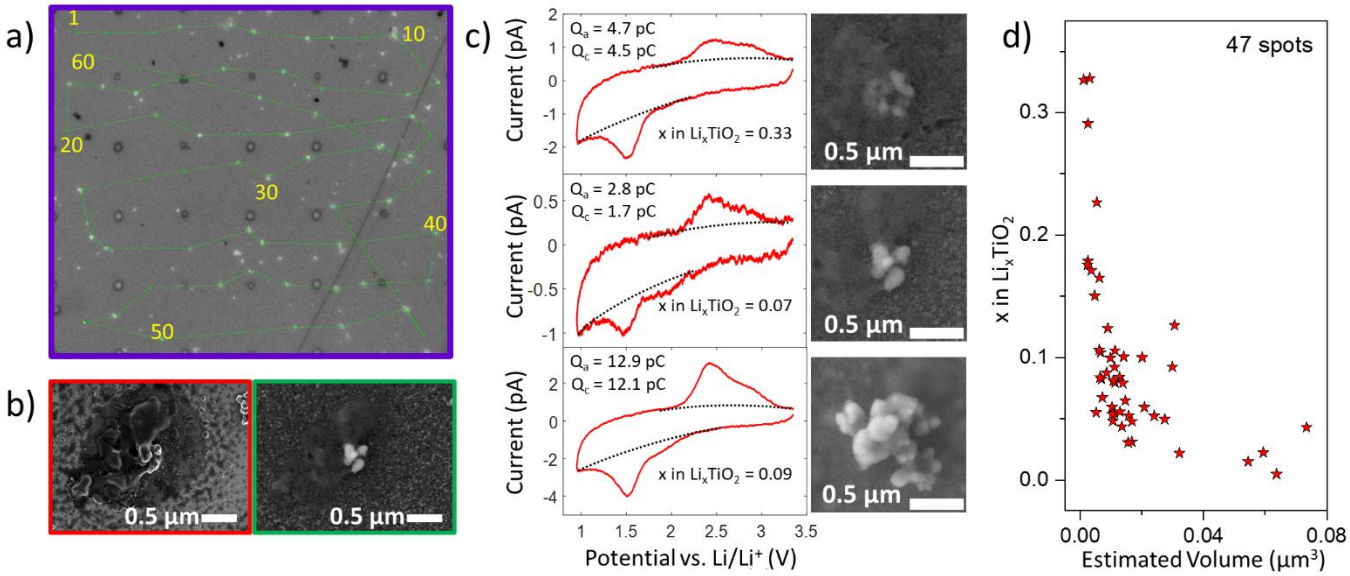

Figure 4. a) IRM image illustrating the calibration scan with 60 points selected as input for automated SECCM measurements with a probe size of 1 µm diameter. b) SEM image of a typical SECCM landing on a TiO_2 nanoparticle cluster recorded by the in-Lens detector (red border) at 1 kV or the Everhart-Thornley (ET) secondary electron detector (green border) at 20 kV. c) CVs at scan rate of 100 mV s^{-1} and corresponding secondary electron ET-SEM images of single TiO_2 nanoparticle clusters. d) Li^+ deintercalation charge as x in Li_xTiO_2 as a function of particle volume calculated for 47 different single TiO_2 nanoparticle clusters.

Scanning electron microscopy with an Everhart-Thornley secondary electron detector (ET-SEM) was used after SECCM measurements to correlate particle features with electrochemical data, while the in-lens detector in SEM highlighted the electrolyte residue left by SECCM (Figure 4b and S17). CVs from selected single TiO_2 nanoparticle clusters and their corresponding ET-SEM images are shown in Figure 4c. The full dataset in Figure S12 and S15 shows remarkably consistent CV responses, with only small variations from cluster to cluster. It is particularly impressive that many CVs show a full current range of < ± 1 pA, with outstanding signal/noise ratio. The Li^+ (de)intercalation capacity was estimated by integrating the charge between the peak currents and a baseline depicted by the dashed lines in Figure 4c to exclude pseudo-capacitive charge storage.

The charge from Li^+ deintercalation (Q_a), which is not compromised by side reactions, was correlated to the particle volume estimated from the ET-SEM image (see section S3 and Figure S18 in SI for volume estimation). Clusters with a smaller volume (i.e. smaller average particle size ~50 nm) and more dispersed on the Au substrate (top panel of Figure 4c) showed higher values of x in Li_xTiO_2 (Figure 4d). Some clusters reached x in Li_xTiO_2 as high as 0.3 at a scan rate of 100 mV s^{-1}, which corresponds to a C-rate above 100 C (see section S4 in SI for C-rate calculation). A small fraction of inserted ions is known to remain in the host lattice of intercalation compounds and cannot be extracted during the first few cycles.[9] Hence, there might be an even higher x for the Li^+ intercalation. This rate performance is at least 10 times superior to those previously reported for specifically-designed TiO_2 materials with ultrafast charging capability,[3,41–45] demonstrating the potential of small commercial TiO_2 particles for fast-charging Li-ion batteries. An increase in particle size (~volume) and agglomeration with a higher particle-particle contact area (middle and bottom panel of Figure 4c) resulted in a decrease in x to less than 0.1, demonstrating the importance of appropriate nanostructuring and bulk electrode engineering to optimise Li^+ intercalation rates.

In conclusion, we have demonstrated fast (de)intercalation of Li^+ in small anatase TiO_2 nanoparticle clusters (30% theoretical capacity at 108 C) and reliably estimated Li^+ diffusivity at the nanoscale (3×10^{-15} cm^2 s^{-1} for Li^+ deintercalation and 2×10^{-14} cm^2 s^{-1} for Li^+ intercalation). This new knowledge may encourage the appropriate engineering of nanostructured anatase electrode that result in a rate performance as close to that demonstrated herein at the single entity level. Our studies have been greatly facilitated by the development of a smart SECCM scanning protocol using *in situ* OM to quickly identify features of interest that are then selected by the user and targeted with the SECCM probe. Smart SECCM drastically reduces the SECCM scan time by more than 90%, while ensuring a much higher probability of landing on particles of interest. This subsequently reduces the risk of tip crash and potential drift of the QRCE and avoids unnecessary computational power for data processing and storage. Given the importance of nanostructures in electrochemical science, we expect smart SECCM to become a powerful tool for high throughput screening, discovery and study of electrochemical materials. The protocol is general and will be applicable to nanoscale point-probe measurements, for a myriad application beyond electromaterials science. A way forward would be the autonomous detection of regions of interest for electrochemical measurement through an intelligent approach (i-SECCM).

Acknowledgements

This project has received funding from the European Union's Horizon 2020 research and innovation programme under the Marie Skłodowska-Curie MSCA-ITN SENTINEL [812398], MSCA-IF NANODENDRITE [101026563] and NanoBat project [861962]. The SECCM-glovebox set-up was funded by the Faraday Institution (FIRG013). We thank Dr. David Walker for helping with XRD measurements, and the use of the XRD Research Technology Platform at the University of Warwick. We

also thank Dr Mark Crouch from the Department of Engineering, University of Warwick, for the fabrication of the gold-coated coverslips.

Conflict of Interest

The authors declare no conflict of interest.

Data Availability Statement

The data that support the findings of this study are openly available in Zenodo at https://doi.org/10.5281/zenodo.7086422.

Keywords: Li-ion battery • Titania • Single particle • Fast charging • Scanning electrochemical cell microscopy

[1] A. J. Merryweather, C. Schnedermann, Q. Jacquet, C. P. Grey, A. Rao, *Nature* **2021**, *594*, 522.
[2] E. Ventosa, T. Löffler, F. La Mantia, W. Schuhmann, *Chem. Commun.* **2016**, *52*, 11524.
[3] M. Fehse, E. Ventosa, *ChemPlusChem* **2015**, *80*, 785.
[4] J. Wang, J. Polleux, J. Lim, B. Dunn, *J. Phys. Chem. C* **2007**, *111*, 14925.
[5] H. Lindström, S. Södergren, A. Solbrand, H. Rensmo, J. Hjelm, A. Hagfeldt, S.-E. Lindquist, *J. Phys. Chem. B* **1997**, *101*, 7717.
[6] Y. Liu, Y. Yang, *J. Nanomater.* **2016**, *2016*, 8123652.
[7] E. Madej, F. La Mantia, W. Schuhmann, E. Ventosa, *Adv. Energy Mater.* **2014**, *4*, 1400829.
[8] T.-H. Kang, B.-J. Lee, C. Lim, H.-Y. Lee, J. W. Han, J.-S. Yu, *ACS Appl. Energy Mater.* **2022**, *5*, 5691.
[9] R. van de Krol, A. Goossens, J. Schoonman, *J. Phys. Chem. B* **1999**, *103*, 7151.
[10] M. Weiss, R. Ruess, J. Kasnatscheew, Y. Levartovsky, N. R. Levy, P. Minnmann, L. Stolz, T. Waldmann, M. Wohlfahrt‐Mehrens, D. Aurbach et al., *Adv. Energy Mater.* **2021**, *11*, 2101126.
[11] R. Borah, F. R. Hughson, J. Johnston, T. Nann, *Mater. Today Adv.* **2020**, *6*, 100046.
[12] D. Martín-Yerga, M. Kang, P. R. Unwin, *ChemElectroChem* **2021**, *8*, 4240.
[13] N. J. J. de Klerk, A. Vasileiadis, R. B. Smith, M. Z. Bazant, M. Wagemaker, *Phys. Rev. Mater.* **2017**, *1,* 025404.
[14] Y.-T. Long, P. R. Unwin, L. A. Baker, *ChemElectroChem* **2018**, *5*, 2918.
[15] E. Ventosa, *Curr. Opin. Electrochem.* **2021**, *25*, 100635.
[16] B. Tao, L. C. Yule, E. Daviddi, C. L. Bentley, P. R. Unwin, *Angew. Chem. Int. Ed.* **2019**, *58*, 4606.
[17] D. Martín‐Yerga, D. C. Milan, X. Xu, J. Fernández‐Vidal, L. Whalley, A. J. Cowan, L. J. Hardwick, P. R. Unwin, *Angew. Chem. Int. Ed.* **2022**, 61, *e202207184*.
[18] C. S. Santos, A. Botz, A. S. Bandarenka, E. Ventosa, W. Schuhmann, *Angew. Chem. Int. Ed.* **2022**, *61*, e202202744.
[19] C. L. Bentley, *Electrochem. Sci. Adv.* **2022**, *2*, e2100081.
[20] O. J. Wahab, M. Kang, P. R. Unwin, *Curr. Opin. Electrochem.* **2020**, *22*, 120.
[21] E. B. Tetteh, T. Löffler, T. Tarnev, T. Quast, P. Wilde, H. B. Aiyappa, S. Schumacher, C. Andronescu, R. D. Tilley, X. Chen et al., *Nano Res.* **2022**, *15*, 1564.
[22] E. B. Tetteh, L. Banko, O. A. Krysiak, T. Löffler, B. Xiao, S. Varhade, S. Schumacher, A. Savan, C. Andronescu, A. Ludwig et al., *Electrochem. Sci. Adv.* **2022**, *2, e2100081*.
[23] Y. Takahashi, A. Kumatani, H. Munakata, H. Inomata, K. Ito, K. Ino, H. Shiku, P. R. Unwin, Y. E. Korchev, K. Kanamura et al., *Nature Comm.* **2014**, *5*, 5450.
[24] C. L. Bentley, M. Kang, P. R. Unwin, *Anal. Chem.* **2020**, *92*, 11673.
[25] Y. Takahashi, T. Yamashita, D. Takamatsu, A. Kumatani, T. Fukuma, *Chem. Commun.* **2020**, *56*, 9324.
[26] D. Valavanis, P. Ciocci, G. N. Meloni, P. Morris, J.-F. Lemineur, I. J. McPherson, F. Kanoufi, P. R. Unwin, *Faraday Discuss.* **2022**, *233*, 122.
[27] P. Saha, J. W. Hill, J. D. Walmsley, C. M. Hill, *Anal. Chem.* **2018**, *90*, 12832.
[28] R. G. Mariano, O. J. Wahab, J. A. Rabinowitz, J. Oppenheim, T. Chen, P. R. Unwin, M. Dincă, *ACS Cent. Sci.* **2022**, *8*, 975.
[29] D. Strmcnik, I. E. Castelli, J. G. Connell, D. Haering, M. Zorko, P. Martins, P. P. Lopes, B. Genorio, T. Østergaard, H. A. Gasteiger et al., *Nat. Catal.* **2018**, *1*, 255.
[30] C. H. Sun, X. H. Yang, J. S. Chen, Z. Li, X. W. Lou, C. Li, S. C. Smith, G. Q. M. Lu, H. G. Yang, *Chem. Commun.* **2010**, *46*, 6129.
[31] J. Liu, J. Wang, C. Xu, H. Jiang, C. Li, L. Zhang, J. Lin, Z. X. Shen, *Adv. Sci.* **2018**, *5*, 1700322.
[32] A. J. Bard, L. R. Faulkner, *Electrochemical Methods: Fundamentals and Applications*, Wiley, New York, **2001**.
[33] J. U. Ha, J. Lee, M. A. Abbas, M. D. Lee, J. Lee, J. H. Bang, *ACS Appl. Mater. Int.* **2019**, *11*, 11391.
[34] M. Wagemaker, R. van de Krol, A. P. Kentgens, A. A. van Well, F. M. Mulder, *J. Am. Chem. Soc.* **2001**, *123*, 11454.
[35] R. Hengerer, L. Kavan, P. Krtil, M. Grätzel, *J. Electrochem. Soc.* **2000**, *147*, 1467.
[36] A. A. Belak, Y. Wang, A. van der Ven, *Chem. Mater.* **2012**, *24*, 2894.
[37] J.-Y. Shin, J. H. Joo, D. Samuelis, J. Maier, *Chem. Mater.* **2012**, *24*, 543.
[38] L. Kavan, J. Rathouský, M. Grätzel, V. Shklover, A. Zukal, *J. Phys. Chem. B* **2000**, *104*, 12012.
[39] L. Kavan, M. Grätzel, S. E. Gilbert, C. Klemenz, H. J. Scheel, *J. Am. Chem. Soc.* **1996**, *118*, 6716.
[40] C. J. Dahlman, S. Heo, Y. Zhang, L. C. Reimnitz, D. He, M. Tang, D. J. Milliron, *J. Am. Chem. Soc.* **2021**, *143*, 8278.
[41] Y. Ren, L. J. Hardwick, P. G. Bruce, *Angew. Chem. Int. Ed.* **2010**, *122*, 2624.
[42] E. Ventosa, A. Tymoczko, K. Xie, W. Xia, M. Muhler, W. Schuhmann, *ChemSusChem* **2014**, *7*, 2584.
[43] Y. Tang, Y. Zhang, J. Deng, J. Wei, H. Le Tam, B. K. Chandran, Z. Dong, Z. Chen, X. Chen, *Adv. Mater.* **2014**, *26*, 6111.
[44] Z. Sun, X. Huang, M. Muhler, W. Schuhmann, E. Ventosa, *Chem. Commun.* **2014**, *50*, 5506.
[45] E. Ventosa, B. Mei, W. Xia, M. Muhler, W. Schuhmann, *ChemSusChem* **2013**, *6*, 1312.

10.1002/anie.202214493

Entry for the Table of Contents

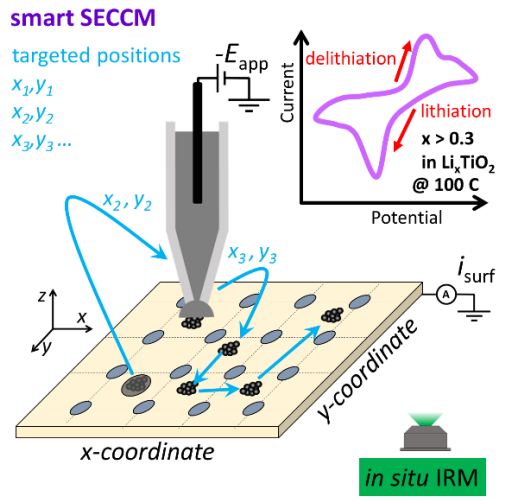

Smart scanning electrochemical cell microscopy (s-SECCM), achieved through *in situ* interference reflection microscopy, enables the high throughput analysis of individual TiO_2 nanoparticle clusters to estimate the Li^+ diffusivity and reveal the inherent fast charging capability of small TiO_2 nanoparticle clusters.

Institute and/or researcher Twitter usernames: @SchuhmannLab, @Warwick_Echem, @ebtetteh, @Patrick_Unwin